J Mater Sci: Mater Electron (2016) 27:304–309
DOI 10.1007/s10854-015-3754-0

Preparation and characterization of the bismuth aluminate nanoparticles via a green approach and its photocatalyst application

Saman Rahnamaeiyan[1] · Ruhollah Talebi[2]

Received: 27 July 2015 / Accepted: 4 September 2015 / Published online: 16 September 2015

Abstract Pure bismuth aluminate ($Bi_2Al_4O_9$) nanoparticles were successfully synthesized by novel sol–gel method with the aid of $Bi(NO_3)_3$, $Al(NO_3)_3{\cdot}9H_2O$, and starch without adding external surfactant, capping agent or template. Moreover, starch plays role as capping agent, reducing agent, and natural template in the synthesis $Bi_2Al_4O_9$ nanoparticles. The structural, morphological and optical properties of as obtained products were characterized by techniques such X-ray diffraction , energy dispersive X-ray microanalysis, scanning electron microscopy, and ultraviolet–visible spectroscopy. The samples indicated a ferromagnetic behavior, as evidenced by using vibrating sample magnetometer at room temperature. To evaluate the photocatalyst properties of nanocrystalline bismuth aluminate, the photocatalytic degradation of methyl orange under ultraviolet light irradiation was carried out.

1 Introduction

In recent years, the preparation of low-dimensional nanostructures has been intensively pursued because of their useful applications in various areas [1–11]. Global industrialization (such as textile, refineries, leather, paper, chemical, and plastic industries) has used different types of dyes resulted in the release of large amounts of toxic compounds into environment [12–17]. Generally, 30–40 % of these dyes remain in the waste waters. Additionally, presence of these dyes diminishes the photosynthesis and causes many serious health problems for humanity. To overcome these problems, the waste water from those industries must be treated before their discharge. Various physical and chemical methods have been used for color removal from waste waters. One of these methods is semiconductor photocatalysis and it has proven to be an effective in treating waste water pollution since it is an environmentally friendly, low-cost, and sustainable treatment methodology [18–22]. The sol gel method of preparing oxide powders generally involves polymerization via hydrolysis and condensation of an alkoxide, gelation, and heat treatment under suitable conditions. In recent years $Bi_2M_4O_9$ ($M = Al^{3+}$, Ga^{3+}, Fe^{3+}) compounds with mullite-type structures [23] have obtained considerable technical interest as potential candidates for applications as oxygen-ion conductors or mixed ionic–electronic conductors (MIEC). Common structural items are chains of edge-shared MO_6 octahedra running parallel to the orthorhombic c-axis linked by (M_2O_7) dimers of MO_4 tetrahedra especially, $Bi_2Al_4O_9$ does not show any phase transition until 1080 °C and has a high chemical stability in hydrogen atmospheres [24, 25], a necessary feature for the application in fuel cells. Tutov and Echerlin described the possibility of orthorhombic bismuth aluminate preparation in 1965 [26–32], as well as defined the synthesis conditions, temperature and melting character of the compound. Among the wet chemical routes, sol–gel technique has been used widely because it has the advantage of producing pure, ultrafine powders at low temperatures, High surface area and pore size distribution [33, 34]. In this report, for the first time, we had presented the preparation of $Bi_2Al_4O_9$ nanoparticles by novel sol–gel method at 800 °C in the

✉ Ruhollah Talebi
ruhollahtalebi90@gmail.com

[1] Young Researchers and Elite Club, Borujerd Branch, Islamic Azad University, Borujerd, Iran

[2] Young Researchers and Elite Club, Central Tehran Branch, Islamic Azad University, Tehran, Iran

presence of starch without adding external surfactant, capping agent or template. A green approach for $Bi_2Al_4O_9$ nanoparticles synthesis by utilizing natural template permits the reaction to proceed usually in milder conditions. Although existing chemical approaches have effectively produced well defined $Bi_2Al_4O_9$ nanoparticles, these processes are generally costly and include the employ of toxic chemicals. The photocatalytic degradation was investigated using methyl orange (MO) under ultraviolet light irradiation.

2 Experimental

2.1 Characterization

Bismuth nitrate pentahydrate $Bi(NO_3)_3.5H_2O$, aluminium nitrate nonahydrate ($Al(NO_3)_3 9H_2O$), were purchased from Merck Company and used without further purification. X-ray diffraction (XRD) patterns were recorded by a Philips-X'PertPro, X-ray diffractometer using Ni-filtered Cu Kα radiation at scan range of $10 < 2\theta < 80$. The electronic spectra of the bismuth aluminate were obtained on a Scinco UV–vis scanning spectrometer (Model S-10 4100). The energy dispersive spectrometry (EDS) analysis was studied by XL30, Philips microscope. Scanning electron microscopy (SEM) images were obtained on LEO-1455VP equipped with an energy dispersive X-ray spectroscopy. The magnetic measurement of samples were carried out in a vibrating sample magnetometer (VSM) (Meghnatis Daghigh Kavir Co.; Kashan Kavir; Iran) at room temperature.

2.2 Synthesis of $Bi_2Al_4O_9$ nanoparticles

At first, 3.41 g of $Bi(NO_3)_3.5H_2O$ was dissolved in 50 mL of distilled water. Then, 8.7 of starch was subsequently added to the above solution under magnetic stirring at 70 °C for 30 min. Afterwards, 5.28 g of $Al(NO_3)_3 9H_2O$ was dissolved in 50 mL of distilled water and was added to the above solution under magnetic stirring. A solution was obtained and further heated at 100 °C for 1 h to remove excess water. During continued heating at 120 °C for 1 h, the solution became more and more viscous to become a gel. Finally, the obtained product was calcinated at 800 °C for 2 h in a conventional furnace in air atmosphere and then cooled it to room temperature.

2.3 Photocatalytic experimental

The methyl orange (MO) photodegradation was examined as a model reaction to evaluate the photocatalytic activities of the bismuth aluminate nanoparticles. The photocatalytic experiments were performed under an irradiation ultraviolet light. The photocatalytic activity of nanocrystalline $Bi_2Al_4O_9$ obtained was studied by the degradation of methyl orange solution as a target pollutant. The photocatalytic degradation was performed with 150 mL solution of methyl orange (0.0005 g) containing 0.05 g of $Bi_2Al_4O_9$. This mixture was aerated for 30 min to reach adsorption equilibrium. Later, the mixture was placed inside the photoreactor in which the vessel was 15 cm away from the visible source of 400 W mercury lamps. The photocatalytic test was performed at room temperature. Aliquots of the mixture were taken at definite interval of times during the irradiation, and after centrifugation they were analyzed by a UV–vis spectrometer. The methyl orange (MO) degradation percentage was calculated as:

$$\text{Degradation rate } (\%) = \frac{A_0 - A}{A_0} \times 100$$

where A_0 and A are the absorbance value of solution at A_0 and A min, respectively.

3 Results and discussion

Figure 1 shows a typical XRD pattern ($10° < 2\theta < 80°$) of $Bi_2Al_4O_9$ nanoparticles. Based on the Fig. 1, the diffraction peaks can be indexed to pure orthorhombic phase of $Bi_2Al_4O_9$ (space group Pbam, JCPDS No. 25-1048). No other crystalline phases were detected. From XRD data, the crystallite diameter (D_c) of $Bi_2Al_4O_9$ nanoparticles was calculated to be 40 nm using the Scherer equation:

$$D_c = K\lambda/\beta\cos\theta \quad \text{Scherer equation}$$

where β is the breadth of the observed diffraction line at its half intensity maximum (400), K is the so-called shape factor, which usually takes a value of about 0.9, and λ is the wavelength of X-ray source used in XRD. The morphology of the nanoparticles was investigated using SEM which demonstrates uniform nanoparticles with spherical shape homogenously distributed all over the sample, as it could be clearly observed in Fig. 2. The $Bi_2Al_4O_9$ nanoparticles with particle size of about 50–55 nm were observed. The EDS analysis measurement was used to investigate the chemical composition and purity of $Bi_2Al_4O_9$ nanoparticles. According to the Fig. 3, the product consists of Bi, Al, and O elements. Furthermore, neither N nor C signals were detected in the EDS spectrum, which means the product is pure and free of any surfactant or impurity. The VSM magnetic measurements for the $Bi_2Al_4O_9$ Fig. 4 show the magnetic properties of nanoparticles calcined at 800 °C. The nanoparticles exhibit ferromagnetic behaviour at room temperature, with a saturation magnetization of .007 emu/g and a coercivity of 75 Oe.

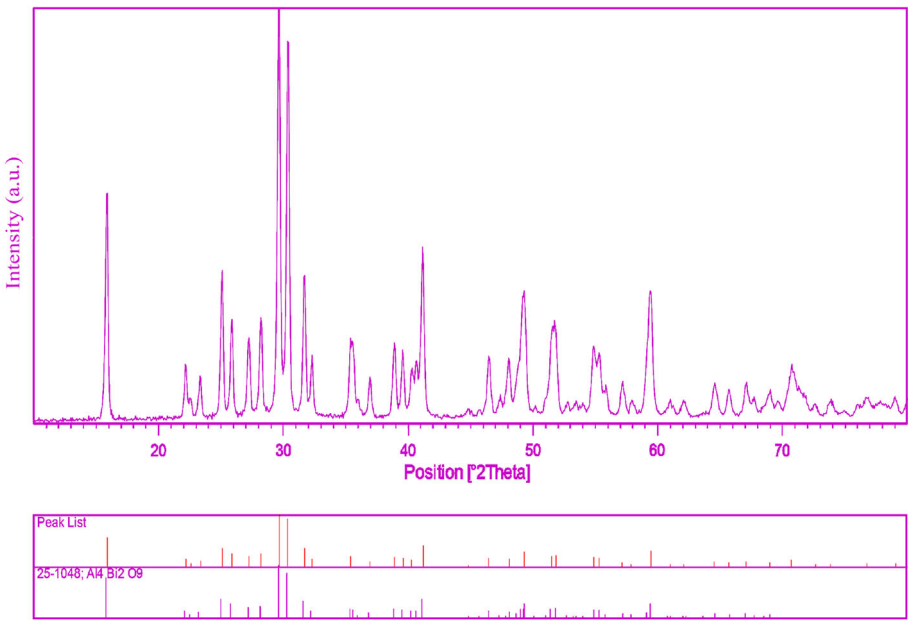

Fig. 1 XRD pattern of $Bi_2Al_4O_9$ nanoparticles calcined at 800 °C

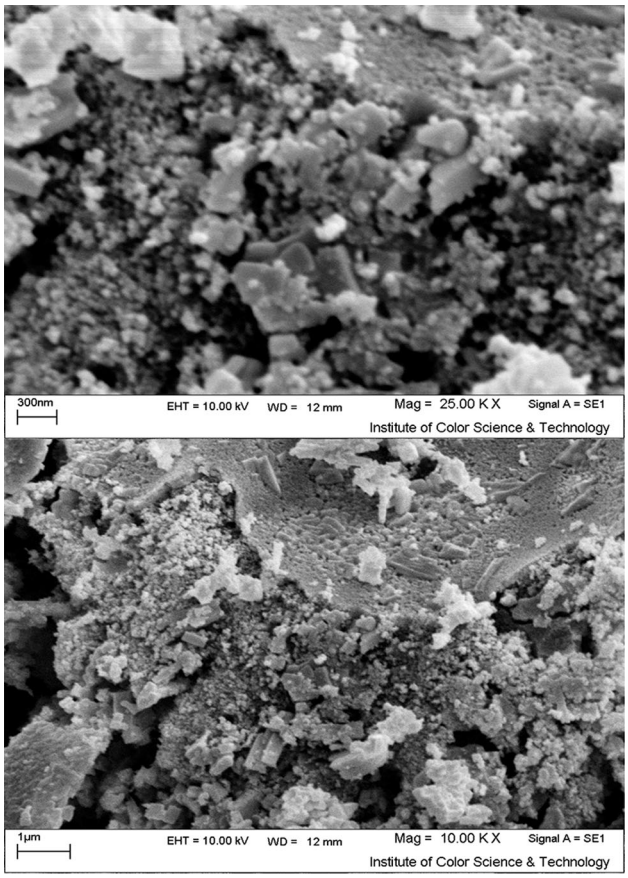

Fig. 2 SEM image of $Bi_2Al_4O_9$ nanoparticles calcined at 800 °C

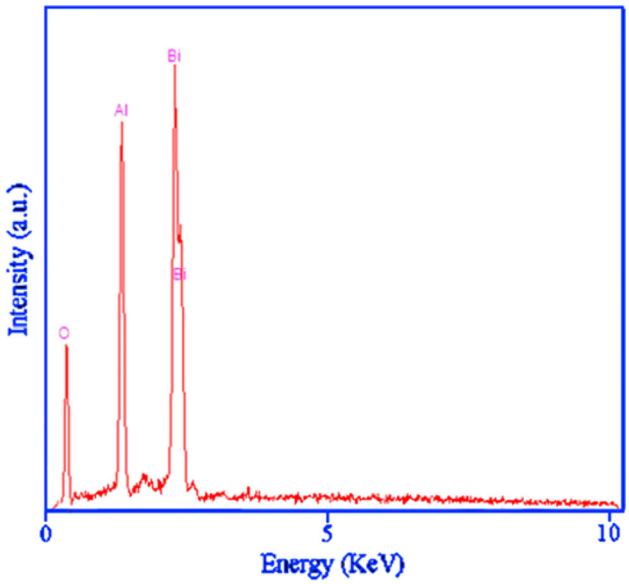

Fig. 3 EDS pattern of $Bi_2Al_4O_9$ nanoparticles calcined at 800 °C

The room temperature UV–vis absorption spectra of $Bi_2Al_4O_9$ nanoparticles were also measured in the range of 300–600 nm. Figure 5a shows the diffuse reflection absorption spectra of the $Bi_2Al_4O_9$ nanoparticles calcinled at 800 °C. The figure indicates that the $Bi_2Al_4O_9$ nanoparticles shows absorption maxima at 373 nm, the direct optical band gap estimated from the absorption spectra for the $Bi_2Al_4O_9$ nanoparticles is shown in Fig. 5b. An optical band gap is obtained by plotting $(\alpha h\nu)^2$ versus $h\nu$ where α is the absorption coefficient and $h\nu$ is photon energy. Extrapolation of the linear portion at $(\alpha h\nu)^2 = 0$ gives the band gaps of 2.8 eV for perovskite $Bi_2Al_4O_9$ material. Photodegradation of methyl orange under UV light irradiation (Fig. 6 a–c) was employed to evaluate the photocatalytic activity of the as-synthesized $Bi_2Al_4O_9$. No

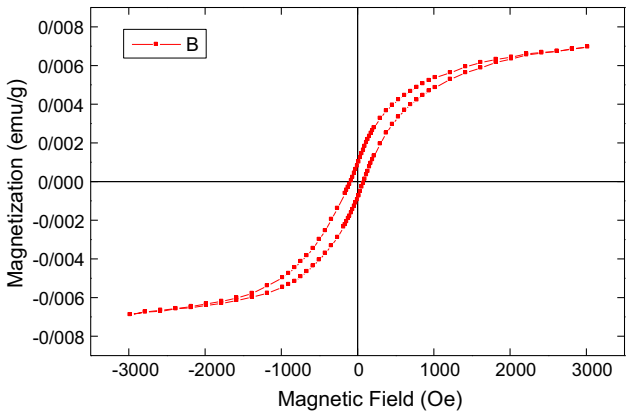

Fig. 4 VSM curves of $Bi_2Al_4O_9$ nanoparticles calcined at 800 °C

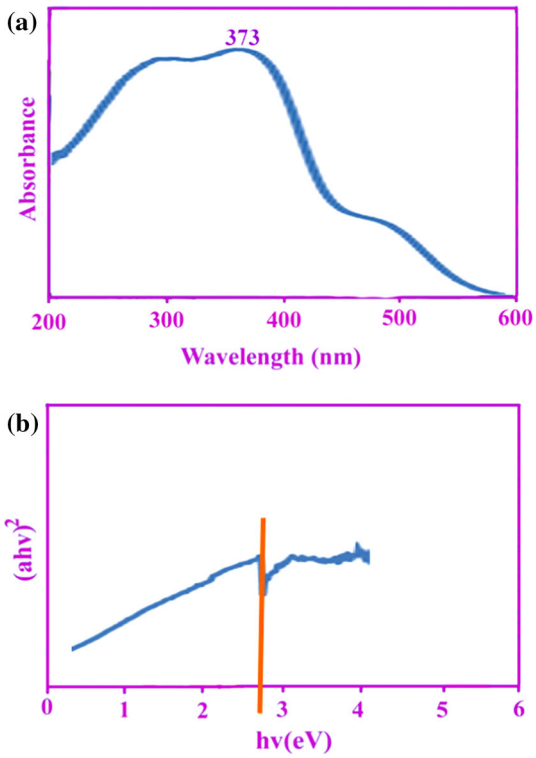

Fig. 5 **a** UV–vis absorption spectra of prepared $Bi_2Al_4O_9$ nanoparticles for 120 min at calcination temperature of 800 °C and **b** plot to determine the direct band gap of $Bi_2Al_4O_9$

methyl orange was practically broken down after 60 min without using UV light irradiation or nanocrystalline $Bi_2Al_4O_9$. This observation indicated that the contribution of self-degradation was insignificant. The probable mechanism of the photocatalytic degradation of methyl orange can be summarized as follows:

$$Bi_2Al_4O_9 + h\nu \rightarrow Bi_2Al_4O_9^{\cdot} + e^- + h^+ \quad (1)$$

$$h^+ + H_2O \rightarrow OH^{\cdot} \quad (2)$$

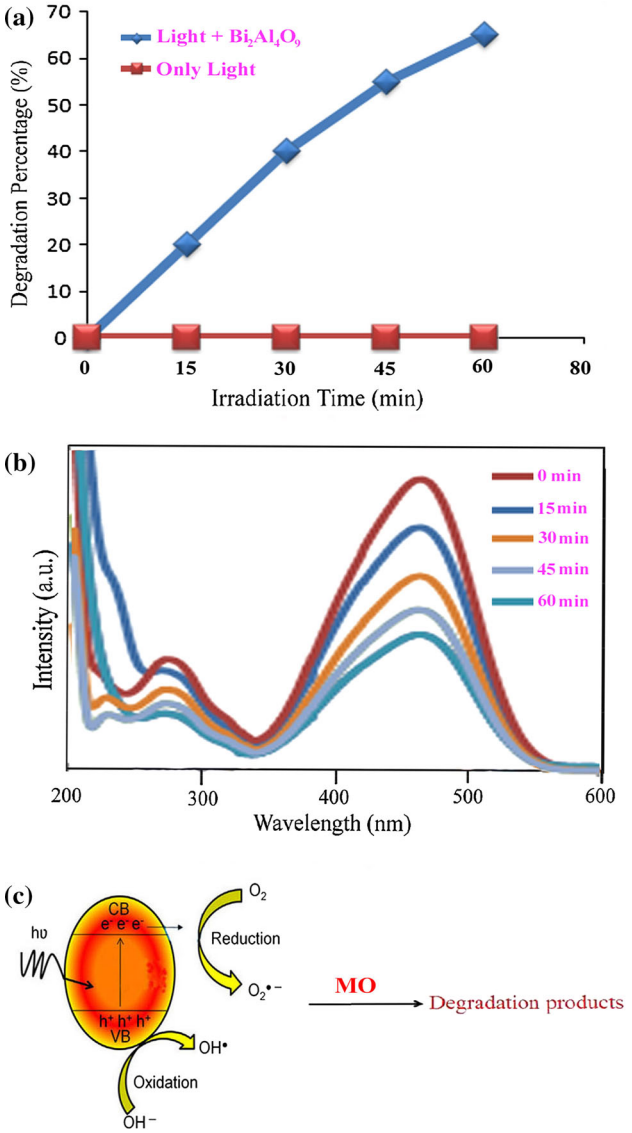

Fig. 6 **a** photocatalytic methyl orange degradation of $Bi_2Al_4O_9$ nanoparticles under ultraviolet light **b** fluorescence spectral time scan of methyl orange illuminated at 510 nm with $Bi_2Al_4O_9$ nanoparticles and **c** reaction mechanism of methyl orange photodegradation over $Bi_2Al_4O_9$ nanoparticles under ultraviolet light irradiation

$$e^- + O_2 \rightarrow O_2^{\cdot -} \quad (3)$$

$$OH^{\cdot} + O_2^{\cdot -} + \text{methyl orange} \rightarrow \text{Degradation products} \quad (4)$$

Using photocatalytic calculations by Eq. (1), the methyl orange degradation was about 65 % after 60 min irradiation of UV light, and nanocrystalline $Bi_2Al_4O_9$ presented high photocatalytic activity (Fig. 6a). The spectrofluorimetric time-scans of methyl orange solution illuminated at 510 nm with nanocrystalline $Bi_2Al_4O_9$ are depicted in Fig. 6b. Figure 6b shows continuous removal of methyl

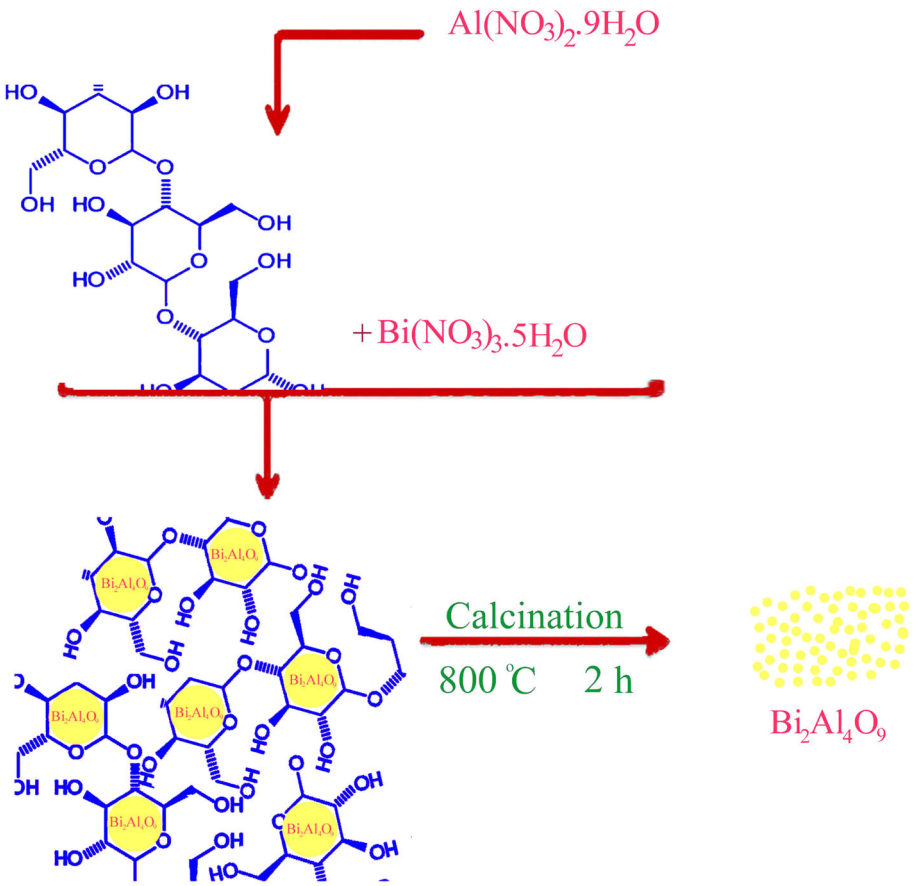

Scheme.1 Schematic diagram illustrating the formation of $Bi_2Al_4O_9$ nanoparticles

orange on the $Bi_2Al_4O_9$ under UV light irradiation. It is generally accepted that the heterogeneous photocatalytic processes comprise various steps (diffusion, adsorption, reaction, and etc.), and suitable distribution of the pore in the catalyst surface is effective and useful to diffusion of reactants and products, which prefer the photocatalytic reaction. In this investigation, the enhanced photocatalytic activity can be related to appropriate distribution of the pore in the sponge-like nanocrystalline $Bi_2Al_4O_9$ surface, high hydroxyl amount and high separation rate of charge carriers 24 (Fig. 6c). Furthermore, this route is facile to operate and very suitable for industrial production of $Bi_2Al_4O_9$ nanoparticles. In addition, this process can be versatile to easily synthesize other titanium based perovskite oxides. The synthesis pathway of $Bi_2Al_4O_9$ nanoparticles is shown in Scheme 1.

4 Conclusions

In this work, bismuth aluminate nanoparticles were successfully synthesized by a novel sol–gel method at 800 °C for 120 min. The stages of the formation of $Bi_2Al_4O_9$, as well as the characterization of the resulting compounds were done using X-ray diffraction and energy dispersive X-ray spectroscopy. The products were analyzed by scanning electron microscopy (SEM), and ultraviolet–visible (UV–Vis) spectroscopy to be round, about 50–55 nm in size and Eg = 2.80 eV. VSM analyzes indicates a ferromagnetic behavior for the synthesized nanoparticles. When as-prepared nanocrystalline bismuth aluminate was utilized as photocatalyst, the percentage of methyl orange degradation was about 65 % after 60 min irradiation of ultraviolet light.

Acknowledgments Authors are grateful to council of University of Central Tehran for providing financial support to undertake this work.

Compliance with ethical standards

Conflict of interest The author declares that the research was conducted in the absence of any commercial or financial relationships that could be construed as a potential conflict of interest.

References

1. M. Ramezani, A. Sobhani-Nasab, A. Davoodi, J. Mater. Sci. Mater. Electron. **26**, 5440 (2015)
2. P. Bakhshaei, A. Ataie, H. Abdizadeh, J. Nanostruct. **3**, 403 (2013)
3. R. Raeisi Shahraki, M. Ebrahimi, J. Nanostruct. **2**, 413 (2013)

4. M. Shakib Nahad, G. Mohammadi Ziarani, A. Badiei, A. Banan, J. Nanostruct. **3**, 395 (2013)
5. M. Rahimi-Nasarabadi, J. Nanostruct. **4**, 211 (2013)
6. M. Najafi, H. Haratizadeh, M. Ghezellou, J. Nanostruct. **5**, 129 (2015)
7. M. Ahmadzadeh, M. Almasi-Kashi, A. Ramazani, J. Nanostruct. **5**, 97 (2015)
8. F.S. Ghoreishi, V. Ahmadi, M. Samadpour, J. Nanostruct. **3**, 453 (2013)
9. S. Moshtaghi, D. Ghanbari, M. Salavati-Niasari, J. Nanostruct. **5**, 169 (2015)
10. A. Rahdar, M. Aliahmad, Y. Azizi, J. Nanostruct. **5**, 145 (2015)
11. J. Safaei-Ghomi, S. Zahedi, M. Javid, M.A. Ghasemzadeh, J. Nanostruct. **5**, 153 (2015)
12. V.B.R. Boppana, D.J. Doren, R.F. Lobo, Chemsuschem. **3**, 814 (2010)
13. K. Gurunathan, J.O. Baeg, S.M. Lee, E. Subramanian, S.J. Moon, K.J. Kong, Int. J. Hydrog. Energ. **33**, 2646 (2008)
14. S.W. Cao, Y.J. Zhu, G.F. Cheng, Y.H. Huang, J. Hazard. Mater. **171**, 431 (2009)
15. T. Debnath, C.H. Rüscher, P. Fielitz, S. Ohmann, G. Borchardt, Ceram. Trans. **217**, 71 (2010)
16. T. Debnath, C.H. Rüscher, ThM Gesing, P. Fielitz, S. Ohmann, G. Borchardt, Ceram. Eng. Sci. Proc. **31**, 81 (2010)
17. J. Maier, B. Bunsenges, J. Phys. Chem. **90**, 26 (1986)
18. J.S. Piccin, C.S. Gomes, L.A. Feris, M. Gutterres, Chem. Eng. J. **183**, 30 (2012)
19. M.N. Chong, B. Jin, C.W.K. Chow, C. Saint, Water Res. **44**, 2997 (2010)
20. A.A. Firooz, A.R. Mahjoub, A.A. Khodadadi, M. Movahedi, Chem. Eng. J. **165**, 735 (2010)
21. D.F. Wang, Z.G. Zou, J.H. Ye, Chem. Phys. Lett. **373**, 191 (2003)
22. Z.R. Zhu, X.Y. Li, Q.D. Zhao, H. Li, Y. Shen, G.H. Chen, Chem. Eng. J. **165**, 64 (2010)
23. H. Schneider, in *Mullite*, ed. by H. Schneider, S. Komarneni (Wiley-VCH, Weinheim, 2005), pp. 141–164
24. T.M. Gesing, C.H. Rüscher, J.C. Buhl, Z. Kristallogr, Z. Kristallogr. Suppl. **29**, 93 (2009)
25. E.I. Speranskaya, V.M. Skorokov, G.M. Safronov, E.N. Gaidukov, Inorg. Mater. **6**, 1201 (1970)
26. A.G. Tutov, I.E. Mylnikova, I.N. Parfenov, V.A. Bokov, Fhisika Tverdogo Tela. **6**, 1240 (1964)
27. P. Eckerlin, J. Liebertz, Naturwissenschaften **52**, 450 (1965)
28. N. Niizeki, M. Wachi, Krist. Bd. **127**, 173 (1968)
29. I. Bloom, M.C. Hash, J.P. Zebrowski, K.M. Myles, M. Krumpelt, Solid State Ionic. **739**, 53 (1992)
30. S. Zha, J. Cheng, Y. Liu, X. Liu, G. Meng, Solid State Ionic. **156**, 197 (2003)
31. S. Larose, S.A. Akbar, J. Solid State Electrochem. **10**, 488 (2006)
32. ThM Gesing, R.X. Fischer, M. Burianek, M. Mühlberg, T. Debnath, J. Ottinger, J.C. Buhl, H. Schneider, J. Eur. Ceram. Soc. **31**, 3055 (2011)
33. H.A. Harwig, A.G. Gerards, J. Solid State Chem. **26**, 265 (1978)
34. K. Laurent, G.Y. Wang, S. Tusseau-Nenez, Y. Leprince-Wang, Solid State Ionic. **178**, 1735 (2008)